Natural Hazards (2019) 99:827–841
https://doi.org/10.1007/s11069-019-03777-z

ORIGINAL PAPER

A fluvially derived flood deposit dating to the Kamikaze typhoons near Nagasaki, Japan

Caroline Ladlow[1] · Jonathan D. Woodruff[1] · Timothy L. Cook[1] · Hannah Baranes[1] · Kinuyo Kanamaru[2]

Received: 26 March 2019 / Accepted: 28 August 2019 / Published online: 4 September 2019

Abstract

Previous studies in western Kyushu revealed prominent marine-derived flood deposits that date to the late thirteenth-century and are interpreted to be a result of two legendary typhoons linked to the failed Mongol invasions of Japan in 1274 and 1281. The regional persistence and prominence of sediments dating to these "Kamikaze" typhoon events (meaning divine wind) raise questions about the origins of these late thirteenth-century deposits. This is due in part to uncertainty in distinguishing between tsunami and storm-induced deposition. To provide additional insight into the true cause of prominent late thirteenth-century flood deposits in western Kyushu, we present a detailed assessment of an additional event deposit dating to the late thirteenth-century from Lake Kawahara near Nagasaki, Japan. This particular deposit thickens landward towards the primary river flowing into Lake Kawahara and exhibits anomalously low Sr/Ti ratios that are consistent with a fluvial rather than a marine sediment source. When combined with previous flood reconstructions, results support the occurrence of an extreme, late thirteenth-century event that was associated with both intense marine- and river-derived flooding. Results therefore contribute to a growing line of evidence for the Kamikaze typhoons resulting in widespread flooding in the region, rather than the late thirteenth-century deposit being associated with a significant tsunami impact to western Kyushu.

Keywords Typhoon · Kamikaze · Kyushu · Overwash deposit · Sediments

Electronic supplementary material The online version of this article (https://doi.org/10.1007/s11069-019-03777-z) contains supplementary material, which is available to authorized users.

✉ Caroline Ladlow
cladlow@umass.edu

[1] Department of Geosciences, University of Massachusetts-Amherst, Amherst, MA, USA

[2] Department of Geology, Amherst College, Amherst, MA, USA

1 Introduction

The shorelines of Japan experience extreme coastal flooding from both seasonal typhoons and episodic tsunami events (Komatsubara and Fujiwara 2007; Sasaki and Yamakawa 2007; Suzuki et al. 2008). Quantifying the spatially-varying risk associated with typhoons and tsunamis across Japan is an essential part of hazard preparation and planning (e.g. Normile 2011; Goslin and Clemmensen 2017); however, this process is challenging because there are inadequate observations of their extremes within temporally-limited instrumental records. There are significant challenges to assessing spatially-varying flood risk from these two separate hazards, due to limited observations of their extremes within short instrumental records (e.g. Goto et al. 2017; Suppasri et al. 2013; Woodruff et al. 2013). Prior to the onset of the best-track dataset of typhoons in the Northern West Pacific in the mid-twentieth century (Chu et al. 2002), one must rely on historical records and natural archives of coastal flooding to constrain flood risk across Japan. The magnitude and impact of the most recent tsunami to strike Japan, the 11 March 2011 Tōhoku tsunami, greatly exceeded prior expectations at the time of the event (Japan Meteorological Agency 2013), underscoring the importance of obtaining additional insight from the historical and geologic record.

Historical documentation of tsunamis and typhoons in Japan extends back at least several 100 years (Nakata and Kawana 1995; Watanabe 2001; Goslin and Clemmensen 2017), but significant uncertainty associated with these early records limits their utility in improving flood risk assessments (Kortekaas and Dawson 2007; Morton et al. 2007). Natural archives of flooding preserved within the geologic record are frequently used to independently validate early historical flood accounts. For example, overwash deposits from high-energy flood events that are preserved within the sedimentary sequences of coastal environments, such as those from back-barrier lakes and marshes, can be used to reconstruct pre-instrumental tsunami and typhoon frequency and intensity (e.g. Komatsubara and Fujiwara 2007; Komatsubara et al. 2008; Chagué-Goff et al. 2012; Wallace et al. 2014; Brandon et al. 2015; Baranes et al. 2016, 2018; Chaumillon et al. 2017). The sandy overwash deposits left by tsunamis and typhoons can often have very similar characteristics including being composed of coarse-grained beach material, exhibiting a lateral thinning landward, and containing elemental signatures consistent with marine-derived sediments. Though it is difficult to unambiguously differentiate between storm and tsunami overwash deposits preserved in back-barrier environments, distinguishing between these types of event layers is important because of the need to separately quantify the risk associated with storms and tsunamis (Nanayama et al. 2000; Kortekaas and Dawson 2007; Morton et al. 2007; Komatsubara et al. 2008; Sawai et al. 2009). Especially in countries like Japan with longer written historical records, pairing event deposits to historical documentation can help circumvent the uncertainty between deposits left by these separate coastal flooding hazards (Nanayama et al. 2000; Goff et al. 2004; Kortekaas and Dawson 2007; Morton et al. 2007; Goto et al. 2015).

The subjectivity of historical accounts of natural disasters often raises questions about their accuracy. For example, legend states that the two failed attempts by the Mongol Empire to invade Japan, first in 1274 and again in 1281, were prevented by the timely intervention of two intense typhoons. Now known as the Kamikaze typhoons, meaning ‘divine wind’, the storms were believed to be an intervention from the gods to protect Japanese sovereignty from the Mongols (Neumann 1975; Rossabi 2009; Sasaki 2015). The historical significance of these typhoons leaves them especially susceptible

to exaggeration over time. The Mongols attributed their failed invasions to the storms, and temples and shrines in Japan highlighted the storms as divine protection of their nation's sovereignty. The occurrence of two intense typhoons striking Japan within only 7 years is also inconsistent with the substantially lower average recurrence rate for typhoon landfalls in the region within the modern instrumental record (Woodruff et al. 2015). Despite the potential for exaggeration and inconsistencies with modern typhoon climatology, natural archives and recent archeological observations support the occurrence of the Kamikaze typhoons. Evidence includes the recent discovery of sunken Mongol ships from the second invasion near Takashima Island in Imari Bay (Kimura et al. 2014; Sasaki 2015) and geologic evidence of contemporaneous overwash deposits in western Kyushu (Woodruff et al. 2009, 2015). Depositional evidence of the Kamikaze typhoons stems from prominent event deposits at Lakes Daija and Kamikoshiki (Fig. 1), with both sites preserving deposits from a marine-sourced flood event consistent with the timing of the two failed Mongol invasions (Woodruff et al. 2009, 2015). A tsunamigenic cause for these deposits could not be ruled out, however, due to similarities in deposition by tsunami- and typhoon-induced coastal flooding. Western Kyushu is largely considered to be at low risk of tsunamis relative to other regions of Japan, but this risk could be greater than current perception should the thirteenth-century deposit

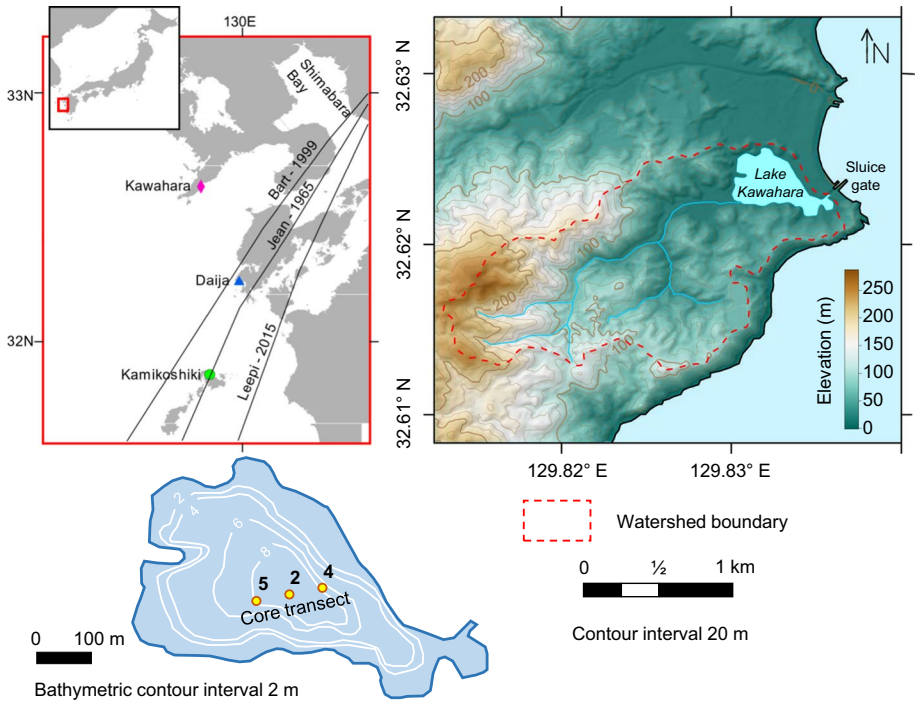

Fig. 1 Top left: Regional map showing the location of Kawahara (diamond), along with other study locations referred to in the text (Daija-triangle, Kamikoshiki-circle), and the paths of best track Category 3 and greater typhoons within 90 km of Lake Kawahara. Top right: Topographic map of Lake Kawahara watershed (brown lines, 20 m contour interval). The primary tributary draining into the lake enters from the southwest, the red dashed line marks the watershed boundary. Bottom left: Bathymetry (2 m contour interval) of Lake Kawahara and numbered core locations (note the order of cores across the transect)

be tsunamigenic in origin. Further research is therefore warranted to both confirm the regional persistence of the late thirteenth-century deposits, as well as to help identify these deposits as either typhoon or tsunamigenic in origin.

Here we present a new sedimentary record from Lake Kawahara, a coastal lake in western Kyushu, to provide further insight regarding the history of extreme flooding in southwestern Japan and the underlying cause of the late thirteenth-century deposits observed at Lake Daija and Kamikoshiki. The Kawahara site is significant because it is sensitive to both coastal overwash and river flooding and provides the potential to use concurrent rainfall-induced river flooding and coastal overwash to delineate typhoon-induced deposition from strictly coastal flooding during tsunami inundation.

2 Site description

Lake Kawahara is a small, coastal, and presently eutrophic lake on the southeast side of the Nagasaki Peninsula, approximately 40 and 80 km north of Lakes Daija and Kamikoshiki, respectively (Fig. 1, 32.62°N, 129.83°E). The lake has a 13 ha (0.013 km^2) surface area, a maximum depth of 9 m, and a thermally stratified water column from February to October each year (Furumoto et al. 1999). A barrier beach forms the seaward side of the lake and is composed of fine to coarse sand and gravel and is approximately 250 m long, 130 m wide, and 7–10 m above mean sea level (MSL). A small inlet through this barrier beach on its southeastern end has resulted in an ephemeral connection between the lake and the ocean. A small high-gradient river empties into the western end of Lake Kawahara and drains a high-relief watershed of 1.4 km^2 with a maximum elevation of 330 m (Fig. 1). The bedrock within the watershed is primarily Cretaceous metamorphic schist, bordered by ultramafic rocks (Geological Survey of Japan 2017). Sea level has remained relatively stable in the region over the past few millennia with a rise of approximately 50 cm since 4100 years BP (Yokoyama et al. 1996, 2012; Sato 2001). The area is also relatively stable tectonically when compared to other regions of Japan closer to active faults (Nakada et al. 1994; Fukumoto 2011).

Since 1945, only three typhoons at or above Category 3 intensity (Simpson and Saffir 1974) have occurred within 90 km of Lake Kawahara: Typhoon Jean in 1965 as a Category 4 storm; Typhoon Bart in 1999 at Category 3 intensity; and Typhoon Leepi in 2015 as a Category 3 event (Fig. 1). Each of these typhoons made landfall to the south of Lake Kawahara, closer to the previously studied Daija and Kamikoshiki sites. No tsunamis have impacted western Kyushu with the exception of a localized tsunami event in 1792 caused by a volcanic dome collapse and resulting landslide internal to Shimabara Bay and located far to the east of the Kawahara site (Hoshizumi et al. 1999) (Fig. 1). The area surrounding the lake has been modified heavily in recent decades in part to mitigate against typhoon impacts. This includes the construction of a seawall that now armors the beach and several jetties near the outlet of the lake. Additionally, Lake Kawahara was historically brackish but a pump was installed in 1974 to remove saltwater from the lake and a sluice gate was installed at the inlet in 1979 (Hossain et al. 2013). Due to coastal fortification and modifications to Lake Kawahara, it is likely that the site is less sensitive to recording coastal flooding within sediments spanning the instrumental period (1945 CE to present); however, the sluice gate and recent pumping of the lake may provide a modern example for the transition from salt to fresh analogous to past natural closures of the barrier beach inlet.

3 Methods

Primary core locations from the deeper part of Lake Kawahara were chosen using bathymetry data collected with a 10 kHz echo-sounder (Kurnio and Aryanto 2010), and subsequently cored using a modified Vohnout–Colinvaux piston corer (Baranes et al. 2016). Initial bathymetric mapping and coring were completed in November 2010, and supplementary surface cores at the same locations were collected in July 2014. Primary cores KAW5 (32.62311°N, 129.832°E), KAW2 (32.62334°N, 129.83264°E), and KAW4 (32.62356°N, 129.83316°E) lie along a shore-normal transect with a spacing of approximately 60–70 m (Fig. 1). Multiple, overlapping drives were collected from each core location in order to recover a continuous sequence. Additional discrete surface sediment samples from the riverbed and the beach were collected to characterize allochthonous sediments from fluvial- and marine-derived sources, respectfully. The beach samples include finer grained material collected around the low-tide mark, and river samples included coarse and fine riverbed sediments and fines in the soil near the riverbank. The central core (KAW2) was selected for constructing a detailed depth-to-age model based on ^{14}C and ^{137}Cs age constraints (Pennington et al. 1973; Ritchie and McHenry 1990; Reimer et al. 2013).

After collection, all cores and discrete surface samples were shipped to the University of Massachusetts (Amherst, MA, USA) and stored at 4 °C. Cores were opened using a Geotek core splitter followed by a complete visual description. Bulk geochemistry of cores and discrete surface samples were evaluated using an ITRAX x-ray fluorescence (XRF) core scanner (Croudace et al. 2006) with a molybdenum (Mo) tube operating at 30 kV and 55 mA and a ten second exposure time. The ITRAX core scanner also provided high-resolution x-radiograph images of relative density, which has proven particularly effective in initially identifying anomalously dense event deposits within cores (e.g. Woodruff et al. 2009, 2015). The ITRAX measures the relative abundances of a wide variety of elements but for the Kawahara cores particular attention was paid to variability in the relative abundance of titanium (Ti), strontium (Sr), and sulfur (S). Ti and Sr are commonly associated with terrigenous (Peterson et al. 2000; Haug et al. 2001; Peterson and Haug 2006) and marine (Bowen 1956; Chen et al. 1997; Chagué-Goff 2010; Croudace and Rothwell 2015) derived sediments, respectively, such that drops and local minima in the ratio of Sr/Ti could potentially represent an increase in terrigenous relative to marine sediment delivery. Elemental sulfur has been used to assess fluctuations in lake salinity associated with past inlet-connectivity to the sea, with higher S indicating higher salinity (Chagué-Goff 2010; Sato 2001; Croudace and Rothwell 2015; Casagrande et al. 1977).

Following scanning with the non-destructive ITRAX core scanner, identified event deposits and background sediments were sub-sampled at 1 cm intervals for grain size. All grain size samples were treated twice with 30% hydrogen peroxide to remove organic material following methods described by Triplett and Heck (2013). Grain sizes were obtained using a Beckman Coulter LS 13 320 laser diffraction particle size analyzer with a range of 0.04–2000 µm.

Ages of recent sediments were determined based on identification of the 1954 onset and 1963 peak in ^{137}Cs activity associated with atmospheric testing of nuclear weapons (Pennington et al. 1973), and measured using a Canberra GL2020R low-energy germanium detector. Age control points below the onset of ^{137}Cs were obtained based on radiocarbon (^{14}C) analysis of terrestrial macrofossils (horizontally oriented leaf material) subsampled from KAW2. Macrofossils were cleaned with deionized water, dried, and shipped to

the National Ocean Science Accelerator Mass Spectrometry (NOSAMS) center in Woods Hole, MA for analysis (Table S1). All provided radiocarbon ages were converted to calendar years BP (years before 1950 CE), using IntCal13 (Reimer et al. 2013). Both the ^{137}Cs and radiocarbon dating results were used to create a Bayesian-derived depth-to-age model with associated uncertainties using the Bchron software package (Haslett and Parnell 2008; Parnell et al. 2008).

4 Results

4.1 Bulk geochemistry of river and beach surface samples

Sr and Ti counts for discrete samples from the barrier beach and primary freshwater stream are evaluated to assess the validity of minima in Sr/Ti as a proxy for terrigenous material enrichment in Lake Kawahara sediments. Ti counts for the river sample were roughly fourteen times that measured for beach sediments, while Sr counts are approximately three times higher in the beach sample than in the river sample (Fig. 2). Therefore, similar to

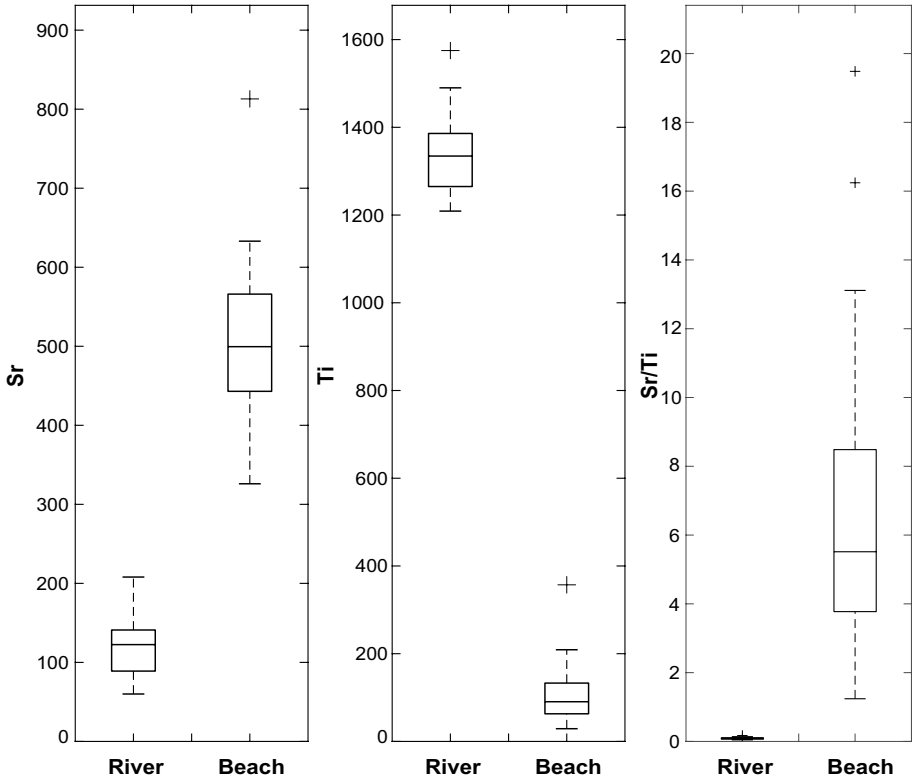

Fig. 2 Relative concentrations of elemental strontium (Sr), titanium (Ti), and the ratio of Sr/Ti in discrete surface samples from the river and beach at Lake Kawahara. Each horizontal line in the box plot marks the 25th, 50th, and 75th percentile, with the whiskers extending to the maximum and minimum values and excluded outliers identified with plus signs

previous results (e.g. Baranes et al. 2016), resultant Sr/Ti ratios are reduced substantially for fluvial-derived material when compared to those with a marine source at Kawahara.

4.2 Visual, physical, and chemical characteristics of sediment cores

The three primary cores KAW5, KAW2, and KAW4 extend to a depth of 377 cm, 540 cm, and 295 cm below the sediment–water interface, respectively. Each core is composed primarily of fine-grained silt and clay, with no sand present, and can be split into three primary lithologic units based on texture, composition, color, and bedding characteristics (Fig. 3). The lower unit in all cores is composed of brown-grey mud and extends from the base of KAW5, KAW2, and KAW4 up to a depth of 245, 280, and 270 (Fig. 3). For the two deeper cores this lower unit contains subunits of darker grey mud at intervals of 260–306 cm in KAW5 and 355–385 cm in KAW2. The intermediate unit in all cores consists of heavily laminated brown-grey mud extending between 150–245 cm, 150–280 cm and 165–270 cm in KAW5, KAW2, and KAW4. This is with the exception of a break in lamination in the intermediate unit in KAW4 between 200 and 245 cm. An upper unit extends from 0 to 150 cm in KAW5 and KAW2, and 0–165 cm in KAW4, and is primarily composed of organic-rich black-grey mud and black gyttja, with a section of laminated muds in between. The upper unit of KAW4 extends down into the brown-grey mud of the intermediate unit, and the delineation between these units is based on the absence of laminations and the decrease in S. The thickness of the uppermost laminated section varies across the transect, from 30 to 40 cm in KAW5 and KAW4, and 30 to 55 cm in

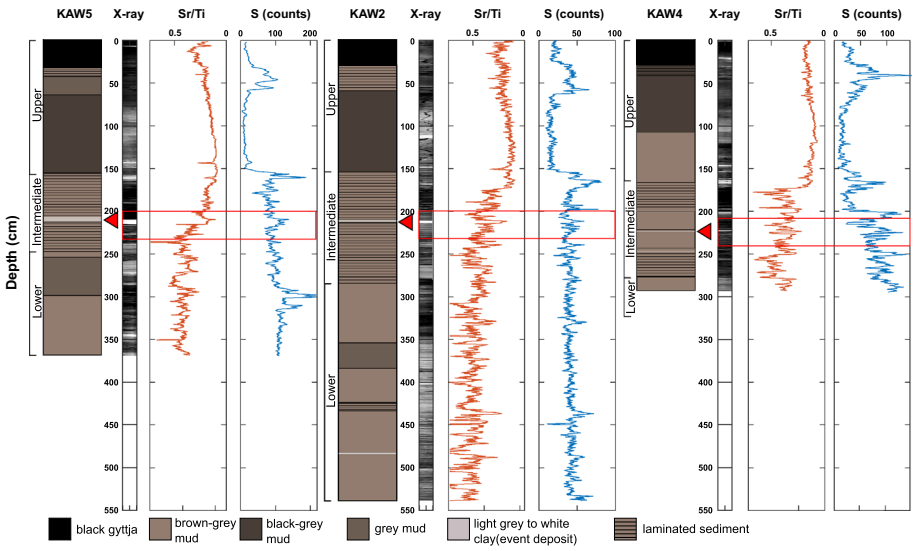

Fig. 3 Depth profiles for the central core transect of KAW5, KAW2, and KAW4 at Lake Kawahara (see Fig. 1 for location). Note the order of cores 5, 2, and 4 go from landward to seaward. From left to right for each core: a graphic core description is pictured with the key below (the upper, intermediate, and lower units of each core are delineated), followed by x-radiograph images with light bands indicating denser sediments, Sr/Ti ratios, and relative abundance of S in total XRF counts. Note that the ratio of Sr/Ti decreases to the right. Triangles in the lithologic sketch identify the densest and most visually prominent event deposit in each core. The red boxes outline the section of the cores shown in Fig. 4

KAW2. Anomalous event deposits in Lake Kawahara appear as high-density layers in the x-radiographs and were also apparent upon visual inspection as light-grey-to-white clay deposits. There is some variability among cores; however, in each core, we focus on the densest and most visually distinct deposit that appears within the intermediate unit, directly below the stratigraphic transition. Our detailed comparison is limited to the intermediate unit due to elemental and stratigraphic evidence that environmental conditions and, in turn, potential sensitivity to flooding has changed above and below this unit. For the three primary cores this deposit is found at varying depths and thicknesses: in KAW5 from 210 to 216 cm (6 cm thick), KAW2 from 212 to 215 cm (3 cm thick), and KAW4 contains avery thin (< 1 cm) deposits from 223 to 224 cm (Fig. 3). The event deposits beginning at 210 cm in KAW5, 212 cm in KAW2, and 223 cm in KAW4 appear correlative based on its location relative to observed stratigraphy and represent a unique, basin-wide depositional event not repeated elsewhere in the record. Across the core transect, median grain sizes in the deposit for inorganic sediments ranged from 15.7 to 19.3 µm and did not exhibit much in terms of distinguishable spatial trends. Clastic material within background sedimentation above and below the deposit were comparable in size, with a median grain sizes range of 15.0 to 31.7 µm (Table 1).

The XRF results for primary core sites exhibit patterns that broadly coincide with the three different lithologic units (Fig. 3). The lower unit has relatively high levels of both S and Sr/Ti that remain fairly constant throughout the unit (note in Fig. 3 that Sr/Ti values increase to the right). There does not appear to be a substantial increase or decrease in S or Sr/Ti at the boundary between the lower unit and intermediate unit, but the top of the intermediate unit shows an up-core decrease in Sr/Ti and a more rapid step-function decrease in S. The transition from the intermediate to upper unit at ~ 150 cm is particularly evident: all cores show a sudden drop in elemental S and a halving in Sr/Ti that begins in the upper portion of the intermediate unit. All three cores also show elevated S abundances that coincide with the heavily laminated sediments both in the intermediate unit, and near the surface at roughly 30–50 cm depth. Following the rise in S at ~ 50 cm in the upper laminated unit there is relatively rapid up-core decline at approximately 30 cm in all three cores and the disappearance of laminations. This transition to unlaminated sediments is followed by a more subtle decrease in Sr/Ti within the uppermost 5–10 cm.

The unique, high-density event deposit at 210 cm in KAW5, 212 cm in KAW2, and 223 cm in KAW4 are all located directly below the rapid up-core drop in S and based on this stratigraphic marker are consistent with being deposited concurrently (Fig. 3). This unique, high-density event deposit identified in all three cores is associated with peaks in S and minima in Sr/Ti (Fig. 4, note similar to Fig. 3 Sr/Ti values increase to the left in Fig. 4). The minima in Sr/Ti is most pronounced in the most landward core KAW5, and observed to become less prominent in relative value for the middle KAW2

Table 1 Grain size results for the background sediments above, below, and within the most prominent event deposit

Core	KAW5 D50 (µm)	KAW2 D50 (µm)	KAW4 D50 (µm)
Above deposit	15.7 ± 1.2 (n = 8)	15.0 ± 1.8 (n = 11)	19.4 ± 4.4 (n = 16)
Deposit	16.9 ± 2.4 (n = 7)	19.3 ± 2.4 (n = 3)	15.7 (n = 1)
Below deposit	15.9 ± 2.0 (n = 15)	15.8 ± 5.0 (n = 16)	31.7 ± 9.6 (n = 13)

The numbers reported are an average of the median (D50) for each sample, the standard deviation of the samples, and n is the number of samples used for each average (a total of 30 samples in each core)

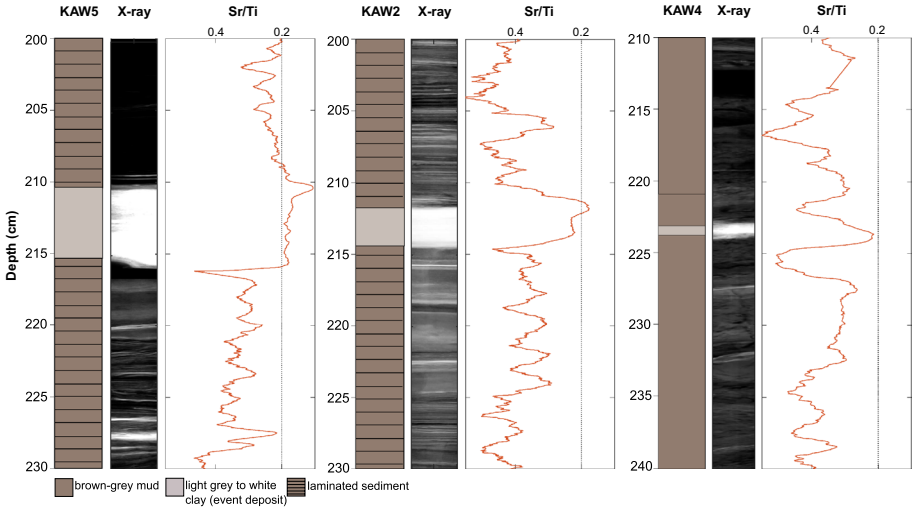

Fig. 4 Left to right: 30 cm section of KAW5, KAW2, and KAW4 surrounding the most notable deposit in each core. Presentation is similar to Fig. 3 showing first the graphic description for each core, followed by the core's x-radiograph and Sr/Ti ratios. The dashed vertical lines in Sr/Ti depth-profiles are all at 0.2 for reference. Note that the ratio of Sr/Ti decreases to the right and that y-axis values are different for each core section. The black lines in the graphic core descriptions are a graphic representation of the laminae rather than the actual lamination counts

core, and followed by the weakest minima in Sr/Ti for the most seaward KAW4 core. A similar seaward decrease is observed in the thickness of this deposit, with a maximum thickness of 6 cm at KAW5, a thickness of 3 cm in KAW2, and a thickness of less than 1 cm in KAW4 (Fig. 4).

4.3 Age model

The five radiocarbon (^{14}C) ages and the modern Cesium (^{137}Cs) age constraints from KAW2 are all chronologically consistent (Fig. 5). Based on ^{14}C ages the 540 cm core extends back to approximately 2500 years BP. The slope of the median age line of the depth-to-age model suggests a relatively steady accumulation rate of 1.5–2.1 mm/year from the base of the core at 540 cm up to the youngest ^{14}C age at 178.5 cm and extending through both the lower and intermediate lithologic units. The accumulation rate increases to approximately 4 mm/year somewhere between the youngest ^{14}C age at 178.5 cm and the onset for ^{137}Cs at 39 cm near the basal extent of the upper lithologic unit. The modern chronological constraints for the onset and peak of ^{137}Cs are consistent with an average accumulation rate of roughly 7 mm/year and are the highest in the core. Applying this modern accumulation rate to recent sediments dates the most up-core recent drop in S at 30 cm to the early 1970s (Fig. 5). The prominent deposit at 212 cm in KAW2 falls within older sediment below the observed rise in accumulation rate above 178.5 cm. The depth-to-age model derived 2-sigma age range for this event deposit is 1155–1487 CE, with a median age of 1321 CE (Fig. 5).

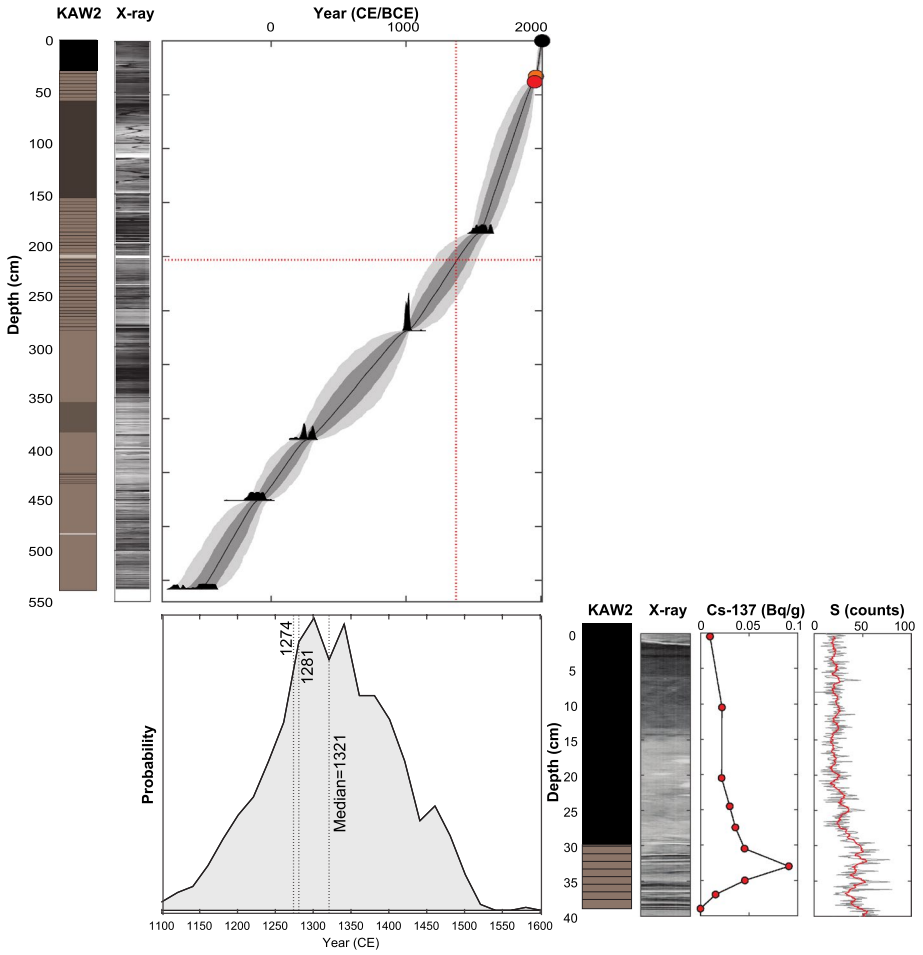

Fig. 5 Left: From left to right: KAW2 core description, radiograph image, and the depth-to-age model constrained by radiocarbon ages (black filled curves) and the onset and peak in ^{137}Cs (red and orange circles, respectively). The black line designates the median age, while the light and dark grey filled regions show the 68 and 95 percent highest posterior density uncertainty ranges. Below left: Age probability distribution for the most prominent event layer at 213 cm. Below right: X-radiograph image of the top 40 cm of KAW2, along with depth profiles of ^{137}Cs activity and S

5 Discussion and interpretation

The transect of cores from Lake Kawahara display three fine-grained lithologic units that likely represent periods of varying degrees of connectivity to the ocean, as shown by the counts of Sr/Ti and S (Fig. 3). The up-core decrease in S at 30 cm (Fig. 5) is concurrent with the installation of the pump and sluice gate in the 1970s to de-salinize the lake, supporting S as a qualitative proxy of salinity in Lake Kawahara, and consistent with past studies (e.g. Croudace and Rothwell 2015; Boyle 2000; Sato 2001; Haug et al. 2003; Chagué-Goff et al. 2012). Additionally, periods of elevated S at Kawahara are largely coincident with the higher preservation of laminations. The lower and intermediate units across

the cores are relatively elevated in Sr/Ti and S, suggesting a more open connection to the ocean during this time and an increased influx of marine-sourced material. The intermediate unit contains the greatest preservation of laminations across all three cores, which is indicative of the salinity-induced stratification of the water column and resulting anoxic bottom waters in the lake. The upper unit of all three cores are relatively depleted in both S and Sr/Ti, which together signify less marine connectivity and an enrichment in fluvial sedimentation relative to marine. The transition between the intermediate and upper units around 1600 CE (~ 150 cm depth) indicates that the inlet was likely closed off to the ocean at this time, cutting off the majority of marine seawater and sediments.

Lake Kawahara sediments lack modern flood deposits for comparison to paleo-deposits (likely due to the fortification of the beach and man-made closure of the barrier inlet in recent decades) and exhibit evidence for sudden shifts in environment and the level of connectivity of the lake to the sea. Both of these factors make it difficult to assemble a complete flood reconstruction through the full 2500-year sedimentary record obtained from the lake. However, the prominent event layer identified in all three cores stands out as a unique depositional event within the lower and intermediate units, which span an interval of 900 years from 1600 to 2500 CE. The high-density signature of this deposit is consistent with it having a higher mineralogic content relative to surrounding sediment, which was potentially sourced from fluvial input of terrestrial material (Fig. 4). The event deposit is also fine-grained (15–19 μm) and thickens landward, which is consistent with flooding from the river (Wright 1977; Cook et al. 2015). In contrast, marine overwash deposits are commonly landward-thinning and coarse-grained (Nanayama et al. 2000; Morton et al. 2007; Komatsubara et al. 2008). Additionally, the cores show that this Kawahara deposit is depleted in Sr/Ti (Fig. 4), which in turn points to an enrichment in fluvial rather than marine sediments (Fig. 2). The KAW2 depth-to-age model reveals that this prominent flood occurred between 1155 and 1487 CE (95% age range) and is consistent with both the timing of the Kamikaze typhoons in 1274 and 1281, and the age of prominent marine overwash deposits previously identified in Lakes Daija and Kamikoshiki. Of the Kamikaze events, the 1281 typhoon is generally considered to be of greater intensity (Turnbull 2013); therefore, we attribute the single late thirteenth-century Kawahara deposit to the later of the two Kamikaze events in 1281 (although it is also possible that the deposit could be combined deposition from the 1274 and 1281 events).

The elemental signature, high density, and landward thickening of the most prominent deposit at Kawahara all support the occurrence of a thirteenth-century extreme precipitation event that overlaps in time with the prominent marine-sourced flood deposits previously identified at Daija and Kamikoshiki. Collectively, these results point to the occurrence of anomalous flooding from both the land and sea during the timing of the failed Mongol invasions, thereby strengthening the evidence for the occurrence of the Kamikaze typhoons. Although the Kamikaze typhoon deposit has a marine signature in Daija and Kamikoshiki, the Lake Kawahara deposit may be fluvial because (1) the barrier at Kawahara is substantially higher (~ 7–10 m) than the barrier beaches at the other two sites (between ~ 2 and 4 m); (2) the watershed of Kawahara is more than double the size of the Kamikoshiki and Daija watersheds; and (3) the 1281 storm track passed between the more northerly Kawahara site and the more southerly Daija and Kamikoshiki sites, such that the front-right quadrant of the storm made landfall over the two southern sites (Landsea et al. 2004; Brandon et al. 2013) and the left side of the storm made landfall over the Kawahara site. In the Northern Hemisphere, the greatest storm surge and coastal flooding tends to occur where the front-right quadrant of a tropical cyclone makes landfall (Emanuel 2005). Therefore, we speculate that if there is more

symmetric precipitation in a storm, a storm deposit is more likely to have a predominantly marine signature in the front-right quadrant, and a fluvial signature in the front left.

Mechanisms other than extreme precipitation exist that could potentially explain the terrestrially derived deposit at Kawahara. For instance, earthquakes accompanying tsunamis could result in landslides that would increase the sediment output from regional rivers (e.g. Milliman and Farnsworth 2011). However, relative to the rest of Japan, the area around Kawahara is depleted in active tsunamigenic faults (Yokoyama et al. 1996; Taira 2001). Further, an enclosed tsunami event generated by local fault sources and localized landslides are unlikely to cause a tsunami large enough in size to impact all three openly seaward-facing sites mentioned in this study. Conversely, a tsunami derived from non-local sources such as the Nankai Trough or the Ryukyu Trench would not be associated with local earthquakes and landslides and in turn would be less likely to result in the terrestrially derived deposit observed at Kawahara. Goto et al. (2017) showed evidence of a tsunami with a return flow back to the sea that resulted in deposition of both fluvial and marine sediments in a lagoon. Thus, a tsunami event of this nature is difficult to rule out completely as the cause of the regional deposit across western Kyushu, despite the evidence of the fluvial deposit observed at Kawahara. However, a tsunami large enough to impact all three sites in western Kyushu would likely have been mentioned in historical records, and no such documentation for a significant tsunami event exists while accounts of the Kamikaze typhoons are prevalent in the region. Thus, the prominent late thirteenth-century fluvial deposit at Kawahara, when combined with historical accounts of the Kamikaze typhoons and previously identified coastal flood deposits at Daija and Kamikoshiki dating to the same time period, all support the Kamikaze typhoons causing significant flooding in the region by both land and sea.

6 Conclusion

Prior results from Lake Daija and Kamikoshiki support the occurrence of late thirteenth-century events associated with extreme coastal flooding in southwestern Kyushu. New analyses presented here from Lake Kawahara provide additional evidence for a late thirteenth-century flood event. The modal age for the most prominent event deposit in Lake Kawahara is matched to the timing of the Mongol invasions, and the deposit can be traced continuously through the obtained transect of cores. However, in contrast to evidence of marine flooding from Lake Daija and Kamikoshiki, the late thirteenth-century deposit at Kawahara thins seaward, shows no significant grain size increase, and exhibits an enrichment in terrigenous material that increases when progressing towards the lake's primary freshwater tributary. The most prominent deposit from Lake Kawahara therefore both dates to the timing of the Mongol invasions and supports significant freshwater flooding during the timing of at least one of the events. When combined with previous regional studies, preserved late thirteenth-century event deposits from near the location of the Mongol invasions in 1274 and 1281 provide evidence for the two leading forms of typhoon-induced flooding (i.e. coastal and fluvial), and in turn contribute to a growing line of evidence for the occurrence of intense typhoons around the time of these invasions.

Acknowledgements Funding and supporting instrumentation were primarily provided by U.S. National Science Foundation (Award #1630090 and Instrument and Facilities Grant #171928).

References

Baranes HE, Woodruff JD, Wallace DJ et al (2016) Sedimentological records of the C.E. 1707 Hōei Nankai Trough tsunami in the Bungo Channel, southwestern Japan. Nat Hazards 84:1185–1205. https://doi.org/10.1007/s11069-016-2498-3

Baranes H, Woodruff JD, Loveless JP, Hyodo M (2018) Interseismic coupling-based earthquake and tsunami scenarios for the Nankai Trough. Geophys Res Lett 45:2986–2994. https://doi.org/10.1002/2018GL077329

Bowen HJM (1956) Strontium and barium in sea water and marine organisms. J Mar Biol As UK 35:451–460. https://doi.org/10.1017/S0025315400010298

Boyle JF (2000) Rapid elemental analysis of sediment samples by isotope source XRF. J Paleolimnol 23:213–221

Brandon CM, Woodruff JD, Lane DP, Donnelly JP (2013) Tropical cyclone wind speed constraints from resultant storm surge deposition: a 2500 year reconstruction of hurricane activity from St. Marks, FL. Geochem Geophys Geosyst 14:2993–3008. https://doi.org/10.1002/ggge.20217

Brandon CM, Woodruff JD, Donnelly JP, Sullivan RM (2015) How unique was Hurricane Sandy? Sedimentary reconstructions of extreme flooding from New York Harbor. Sci Rep. https://doi.org/10.1038/srep07366

Casagrande DJ, Siefert K, Berschinski C, Sutton N (1977) Sulfur in peat-forming systems of the Okefenokee Swamp and Florida Everglades: origins of sulfur in coal. Geochim Cosmochim Acta 41:161–167. https://doi.org/10.1016/0016-7037(77)90196-X

Chagué-Goff C (2010) Chemical signatures of palaeotsunamis: a forgotten proxy? Mar Geol 271:67–71. https://doi.org/10.1016/j.margeo.2010.01.010

Chagué-Goff C, Andrew A, Szczuciński W et al (2012) Geochemical signatures up to the maximum inundation of the 2011 Tohoku-oki tsunami—implications for the 869AD Jogan and other palaeotsunamis. Sed Geol 282:65–77. https://doi.org/10.1016/j.sedgeo.2012.05.021

Chaumillon E, Bertin X, Fortunato AB et al (2017) Storm-induced marine flooding: lessons from a multidisciplinary approach. Earth Sci Rev 165:151–184. https://doi.org/10.1016/j.earscirev.2016.12.005

Chen Z, Chen Z, Zhang W (1997) Quaternary stratigraphy and trace-element indices of the Yangtze Delta, Eastern China, with special reference to marine transgressions. Quatern Res 47:181–191. https://doi.org/10.1006/qres.1996.1878

Chu J-H, Sampson CR, Levine AS, Fukada E (2002) The joint typhoon warning center tropical cyclone best-tracks, 1945–2000. Ref NRL/MR/754002, vol 16

Cook TL, Yellen BC, Woodruff JD, Miller D (2015) Contrasting human versus climatic impacts on erosion. Geophys Res Lett 42:6680–6687. https://doi.org/10.1002/2015GL064436

Croudace IW, Rothwell RG (2015) Micro-XRF studies of sediment cores. Springer, Berlin

Croudace IW, Rindby A, Rothwell RG (2006) ITRAX: description and evaluation of a new multi-function X-ray core scanner. Geol Soc Lond Spec Publ 267:51–63. https://doi.org/10.1144/GSL.SP.2006.267.01.04

Emanuel K (2005) Increasing destructiveness of tropical cyclones over the past 30 years. Nature 436:686–688. https://doi.org/10.1038/nature03906

Fukumoto Y (2011) Mid-late Holocene paleoenvironment in Karako lowland, western Japan, inferred from diatom analysis. Quatern Int 230:115–121. https://doi.org/10.1016/j.quaint.2010.08.003

Furumoto K, Takemoto Y, Makita H, Tateishi H (1999) The change of the water quality and nutrient release from bottom sediment in Kawahara Lake. Proc Hydraul Eng 43:1001–1006. https://doi.org/10.2208/prohe.43.1001

Geological Survey of Japan (2017) Online geological map of Japan. https://www.gsj.jp/en/education/geomap-e/online-map.html. Accessed 30 Jan 2019

Goff J, McFadgen BG, Chagué-Goff C (2004) Sedimentary differences between the 2002 Easter storm and the 15th-century Okoropunga tsunami, southeastern North Island, New Zealand. Mar Geol 204:235–250. https://doi.org/10.1016/S0025-3227(03)00352-9

Goslin J, Clemmensen LB (2017) Proxy records of Holocene storm events in coastal barrier systems: storm-wave induced markers. Quatern Sci Rev 174:80–119. https://doi.org/10.1016/j.quascirev.2017.08.026

Goto T, Satake K, Sugai T et al (2015) Historical tsunami and storm deposits during the last five centuries on the Sanriku coast, Japan. Mar Geol 367:105–117. https://doi.org/10.1016/j.margeo.2015.05.009

Goto T, Satake K, Sugai T et al (2017) Effects of topography on particle composition of 2011 tsunami deposits on the ria-type Sanriku coast, Japan. Quatern Int 456:17–27. https://doi.org/10.1016/j.quaint.2017.05.014

Haslett J, Parnell A (2008) A simple monotone process with application to radiocarbon-dated depth chronologies. J Roy Stat Soc: Ser C (Appl Stat) 57:399–418

Haug GH, Hughen KA, Sigman DM et al (2001) Southward migration of the intertropical convergence zone through the Holocene. Science 293:1304–1308. https://doi.org/10.1126/science.1059725

Haug GH, Günther D, Peterson LC et al (2003) Climate and the collapse of Maya civilization. Science 299:1731–1735. https://doi.org/10.1126/science.1080444

Hoshizumi H, Uto K, Watanabe K (1999) Geology and eruptive history of Unzen volcano, Shimabara Peninsula, Kyushu, SW Japan. J Volcanol Geoth Res 89:81–94. https://doi.org/10.1016/S0377-0273(98)00125-5

Hossain MdM, Perhar G, Arhonditsis GB et al (2013) Examination of the effects of largemouth bass (*Micropterus salmoides*) and bluegill (*Lepomis macrochirus*) on the ecosystem attributes of lake Kawahara-oike, Nagasaki, Japan. Ecol Inf 18:149–161. https://doi.org/10.1016/j.ecoinf.2013.07.005

Japan Meteorological Agency (2013) Lessons learned from the tsunami disaster caused by the 2011 Great East Japan Earthquake and improvements in JMA's tsunami warning system

Kimura J, Staniforth M, Lien LT, Sasaki R (2014) Naval battlefield archaeology of the lost Kublai Khan fleets: naval battlefield archaeology of the Kublai Khan fleets. Int J Naut Archaeol 43:76–86. https://doi.org/10.1111/1095-9270.12033

Komatsubara J, Fujiwara O (2007) Overview of Holocene tsunami deposits along the Nankai, Suruga, and Sagami Troughs, southwest Japan. In: Satake K, Okal EA, Borrero JC (eds) Tsunami and its hazards in the Indian and Pacific Oceans. Birkhäuser, Basel, pp 493–507

Komatsubara J, Fujiwara O, Takada K et al (2008) Historical tsunamis and storms recorded in a coastal lowland, Shizuoka Prefecture, along the Pacific Coast of Japan. Sedimentology 55:1703–1716. https://doi.org/10.1111/j.1365-3091.2008.00964.x

Kortekaas S, Dawson AG (2007) Distinguishing tsunami and storm deposits: an example from Martinhal, SW Portugal. Sed Geol 200:208–221. https://doi.org/10.1016/j.sedgeo.2007.01.004

Kurnio H, Aryanto NCD (2010) Paleo-channels of Singkawang waters west Kalimantan and its relation to the occurrences of sub-seabot tom gold placers based on strata box seismic record analyses. Bull Mar Biol 25:12

Landsea CW, Anderson C, Charles N et al (2004) The Atlantic hurricane database re-analysis project: documentation for the 1851–1910 alterations and additions to the HURDAT database. In: Murnane R, Liu K (eds) Hurricanes and typhoons: past, present and future. Columbia University Press, New York, pp 177–221

Milliman JD, Farnsworth KL (2011) Runoff, erosion, and delivery to the coastal ocean. River discharge to the coastal ocean: a global synthesis. Cambridge University Press, Cambridge, pp 13–69

Morton RA, Gelfenbaum G, Jaffe BE (2007) Physical criteria for distinguishing sandy tsunami and storm deposits using modern examples. Sed Geol 200:184–207. https://doi.org/10.1016/j.sedgeo.2007.01.003

Nakada M, Maeda Y, Nagaoka S et al (1994) Glacio-hydro-isostasy and underwater Jomon sites along the West Coast of Kyushu, Japan. Quat Res 33:361–368. https://doi.org/10.4116/jaqua.33.361

Nakata T, Kawana T (1995) Historical and prehistorical large tsunamis in the southern Ryukyus, Japan. In: Tsuchiya Y, Shuto N (eds) Tsunami: progress in prediction, disaster prevention and warning. Springer, Dordrecht, pp 211–221

Nanayama F, Shigeno K, Satake K et al (2000) Sedimentary differences between the 1993 Hokkaido-nanseioki tsunami and the 1959 Miyakojima typhoon at Taisei, southwestern Hokkaido, northern Japan. Sed Geol 135:255–264. https://doi.org/10.1016/S0037-0738(00)00076-2

Neumann J (1975) great historical events that were significantly affected by the weather: I. the Mongol invasions of Japan. Bull Am Meteor Soc 56:1167–1171. https://doi.org/10.1175/1520-0477(1975)056%3c1167:GHETWS%3e2.0.CO;2

Normile D (2011) Scientific consensus on great quake came too late. Science 332:22–23. https://doi.org/10.1126/science.332.6025.22

Parnell AC, Haslett J, Allen JRM et al (2008) A flexible approach to assessing synchroneity of past events using Bayesian reconstructions of sedimentation history. Quatern Sci Rev 27:1872–1885. https://doi.org/10.1016/j.quascirev.2008.07.009

Pennington W, Tutin TG, Cambray RS, Fisher EM (1973) Observations on lake sediments using fallout 137Cs as a tracer. Nature 242:324–326. https://doi.org/10.1038/242324a0

Peterson LC, Haug GH (2006) Variability in the mean latitude of the Atlantic Intertropical Convergence Zone as recorded by riverine input of sediments to the Cariaco Basin (Venezuela). Palaeogeogr Palaeoclimatol Palaeoecol 234:97–113. https://doi.org/10.1016/j.palaeo.2005.10.021

Peterson LC, Haug GH, Hughen KA, Röhl U (2000) Rapid changes in the hydrologic cycle of the tropical Atlantic during the last glacial. Science 290:1947–1951. https://doi.org/10.1126/science.290.5498.1947

Reimer PJ, Bard E, Bayliss A et al (2013) IntCal13 and Marine13 radiocarbon age calibration curves 0–50,000 years cal BP. Radiocarbon 55:1869–1887. https://doi.org/10.2458/azu_js_rc.55.16947

Ritchie JC, McHenry JR (1990) Application of radioactive fallout cesium-137 for measuring soil erosion and sediment accumulation rates and patterns: a review. J Environ Qual 19:215–233. https://doi.org/10.2134/jeq1990.00472425001900020006x
Rossabi M (2009) Khubilai Khan: his life and times. Univ of California Press, Berkley
Sasaki RJ (2015) The origins of the lost fleet of the Mongol Empire. Texas A&M University Press, College Station
Sasaki H, Yamakawa S (2007) Natural hazards in Japan. In: Lidstone J, Dechano LM, Stoltman JP (eds) International perspectives on natural disasters: occurrence, mitigation, and consequences. Springer, Dordrecht, pp 163–180
Sato H (2001) Holocene uplift derived from relative sea-level records along the coast of western Kobe, Japan. Quatern Sci Rev 20:1459–1474. https://doi.org/10.1016/S0277-3791(01)00005-1
Sawai Y, Kamataki T, Shishikura M et al (2009) Aperiodic recurrence of geologically recorded tsunamis during the past 5500 years in eastern Hokkaido, Japan. J Geophys Res Solid Earth. https://doi.org/10.1029/2007JB005503
Simpson RH, Saffir H (1974) The hurricane disaster potential scale. Weatherwise 27(8):169
Suppasri A, Shuto N, Imamura F et al (2013) Lessons learned from the 2011 Great East Japan tsunami: performance of tsunami countermeasures, coastal buildings, and tsunami evacuation in Japan. Pure appl Geophys 170:993–1018. https://doi.org/10.1007/s00024-012-0511-7
Suzuki A, Yokoyama Y, Kan H et al (2008) Identification of 1771 Meiwa tsunami deposits using a combination of radiocarbon dating and oxygen isotope microprofiling of emerged massive Porites boulders. Quat Geochronol 3:226–234. https://doi.org/10.1016/j.quageo.2007.12.002
Taira A (2001) Tectonic evolution of the Japanese Island arc system. Annu Rev Earth Planet Sci 29:109–134. https://doi.org/10.1146/annurev.earth.29.1.109
Triplett L, Heck J (2013) LacCore grain size pretreatment SOP
Turnbull S (2013) The Mongol invasions of Japan 1274 and 1281. Bloomsbury Publishing, London
Wallace DJ, Woodruff JD, Anderson JB, Donnelly JP (2014) Palaeohurricane reconstructions from sedimentary archives along the Gulf of Mexico, Caribbean Sea and western North Atlantic Ocean margins. Geol Soc Lond Spec Publ 388:481–501. https://doi.org/10.1144/SP388.12
Watanabe H (2001) Is it possible to clarify the real state of past earthquakes and tsunamis on the basis of legends? As an example of the 869 Jogan earthquake and tsunami. Hist Earthq 17:130–146
Woodruff JD, Donnelly JP, Okusu A (2009) Exploring typhoon variability over the mid-to-late Holocene: evidence of extreme coastal flooding from Kamikoshiki, Japan. Quatern Sci Rev 28:1774–1785. https://doi.org/10.1016/j.quascirev.2009.02.005
Woodruff JD, Irish JL, Camargo SJ (2013) Coastal flooding by tropical cyclones and sea-level rise. Nature 504:44–52. https://doi.org/10.1038/nature12855
Woodruff JD, Kanamaru K, Kundu S, Cook TL (2015) Depositional evidence for the Kamikaze typhoons and links to changes in typhoon climatology. Geology 43:91–94. https://doi.org/10.1130/G36209.1
Wright LD (1977) Sediment transport and deposition at river mouths: a synthesis. GSA Bull 88:857–868. https://doi.org/10.1130/0016-7606(1977)88%3c857:STADAR%3e2.0.CO;2
Yokoyama Y, Nakada M, Maeda Y et al (1996) Holocene sea-level change and hydro-isostasy along the west coast of Kyushu, Japan. Palaeogeogr Palaeoclimatol Palaeoecol 123:29–47. https://doi.org/10.1016/0031-0182(95)00112-3
Yokoyama Y, Okuno J, Miyairi Y et al (2012) Holocene sea-level change and Antarctic melting history derived from geological observations and geophysical modeling along the Shimokita Peninsula, northern Japan: Holocene sea level and antarctic melting. Geophys Res Lett 39:1–2. https://doi.org/10.1029/2012gl051983